# Effect of physical activation/surface functional groups on wettability and electrochemical performance of carbon/activated carbon aerogels based electrode materials for electrochemical capacitors

Abbas, Qaisar; Mirzaeian, Mojtaba; Ogwu, Abraham A.; Mazur, Michal; Gibson, Des

*Published in:*
International Journal of Hydrogen Energy

*DOI:*
10.1016/j.ijhydene.2018.04.099

Published: 07/05/2020

*Document Version*
Peer reviewed version

# Effect of physical activation / surface functional groups on wettability and electrochemical performance of carbon / activated carbon aerogels based electrode materials for electrochemical capacitors

*Qaisar Abbas [a*], Mojtaba Mirzaeian [a], Abraham A Ogwu [a], Michal Mazur [b] and Des Gibson [a]*

[a] School of Engineering and Computing, University of the West of Scotland, Paisley PA1 2BE, United Kingdom.

[b] Wroclaw University of Science & Technology, Faculty of Microsystem Electronics and Photonics, Janiszewskiego 11/17, 50-372 Wroclaw, Poland

Corresponding author e-mail address: qaisar.abbas@uws.ac.uk

## Abstract

Polymeric carbon / activated carbon aerogels were synthesized through sol-gel polycondensation reaction followed by the carbonization at 800 ºC under Argon (Ar) atmosphere and subsequent physical activation under $CO_2$ environment at different temperatures with different degrees of burn-off. Significant increase in BET specific surface area (SSA) from 537 to 1775 $m^2g^{-1}$ and pore volume from 0.24 to 0.94 $cm^3g^{-1}$ was observed after physical activation while the pore size remained constant (around 2nm). Morphological characterization of the carbon and activated carbons was conducted using X-ray diffraction (XRD) and Raman spectroscopy. Fourier-transform infrared spectroscopy (FTIR) and X-ray photoelectron spectroscopy (XPS) were used to investigate the effect of thermal treatment (surface cleaning) on the chemical composition of carbon samples.

Cyclic voltammetry (CV) and electrochemical impedance spectroscopy (EIS) were used to analyse the capacitive and resistive behaviour of non-activated/ activated/ and surface cleaned activated carbons employed as electroactive material in a two electrode symmetrical electrochemical capacitor (EC) cell with 6M KOH solution used as the electrolyte.

CV measurements showed improved specific capacitance (SC) of 197 $Fg^{-1}$ for activated carbon as compared to the SC of 136 $Fg^{-1}$ when non-activated carbon was used as electroactive material at a scan rate of 5$mVs^{-1}$. Reduction in SC from 197 $Fg^{-1}$ to 163 $Fg^{-1}$ was witnessed after surface cleaning at elevated temperatures due to the reduction of surface oxygen function groups.

The result of EIS measurements showed low internal resistance for all carbon samples indicating that the polymeric carbons possess a highly conductive three dimensional crosslinked structure. Because of their preferred properties such as controlled porosity, exceptionally high specific surface area, high conductivity and desirable capacitive behaviour, these materials have shown potential to be adopted as electrode materials in electrochemical capacitors.

## Keywords

Carbon aerogels, Surface functional groups, Physical activation, Cyclic voltammetry (CV), Electrochemical capacitors (EC's), electrochemical impedance spectrometry (EIS)

**Abbreviations**

| | |
|---|---|
| EC | Electrochemical capacitor |
| CV | Cyclic voltammetry |
| EIS | Electrochemical impedance spectroscopy |
| SC | Specific capacitance |
| EDLC | Electric double layer capacitor |
| PC | Pseudocapacitor |
| RC | Redox supercapacitor |
| R | Resorcinol |
| F | Formaldehyde |
| SSA | Specific surface area |
| PSD | Pore size distribution |
| XRD | X-ray diffraction |
| FTIR | Fourier-transform infrared spectroscopy |
| XPS | X-ray photoelectron spectroscopy |
| BET | Brunauer–Emmett–Teller |
| Sur-C | Surface cleaned |

## 1. Introduction

With continuous increase in the contribution of renewable energies to the global energy demands, energy conversion / storage systems such as fuel cells [1-3], batteries [4] and electrochemical capacitors (EC's) [5] have attracted considerable research interest in recent years. Due to their advantageous properties such as superior power capability [6], good cycle ability [7] and excellent charge / discharge competency [8], additional emphasis has been placed on research and development of EC's also known as supercapacitors or ultracapacitors. Charge storage mechanism of EC's can be divided into two main categories termed as electric double layer capacitors (EDLC's) and pseudocapacitors (PC's) or redox supercapacitors (RC's). EDLC's are the most frequently used devices where electrical charge is stored electrostatically on electrode / electrolyte interface, whereas charge storage in PC's is based on very fast and fully reversible redox reactions at the interface [9]. The application of ECs have diversified in recent years with being used as a standalone device in applications concerning energy capture and reuse and being adopted as complimentary device alongside other electrochemical energy storage devices in applications such as hybrid electrical vehicles and uninterruptible power supply [10-12]. Despite their fast charge/discharge capability and high power densities, inferior energy density of ECs in comparison with other electrochemical energy storage devices such as fuel cells and electrochemical batteries is considered as a key limitation for their application as main stream energy storage devices. Increasing the operating voltage or the specific capacitance is considered as common strategy to improve the energy density of EC's. Operating voltage of an EC can be enhanced by adopting non-aqueous solutions such as organic [13] or ionic liquids [14, 15] as electrolyte. Whereas, its specific capacitance can be improved by increasing the electrochemical active surface area [16] and controlling the porosity of electroactive material [17, 18], increasing the electrode / electrolyte wettability [19] or by the incorporation of pseudocapacitive components within its electrodes [20]. ECs with higher specific capacitance are developed by combining pseudo-capacitance with electric double layer capacitance through the introduction of pseudocapacitive materials such as metal oxides, conducting polymers or nitrogen / oxygen functional groups within the structure of porous carbons. Electric double layer capacitance is contributed by interfacial electrostatic charges storage using porous activated carbon with optimised porosity and pseudo-capacitance is realized due to the incorporation of metal oxides such as ZnO [21] or $MnO_2$ [22] into the bulk of carbon material or as a result of surface functional groups originated by the introduction of nitrogen or oxygen heteroatoms on the surface of carbon material.

Presence of heteroatoms in highly porous activated carbon can improve the capacitance due to the reversible redox reaction of oxygen / nitrogen functional groups since oxygen and nitrogen functional groups are electron-acceptors and electron-donners respectively [23, 24]. Functional groups also change the surface chemistry which increases the wettability of electrode-electrolyte interface with the formation of polar functional groups [19]. Electrode materials based on carbon such as carbon nanotubes , graphene and activated carbon are the most commonly adopted electrode materials for EC's [25]. Due to their high specific surface area, high level of porosity ,controllable pore size during their synthesis, high electric conductivity, inertness and interconnected microstructure activated carbons obtained by the pyrolysis and activation of polymeric aerogels are used for variety of applications such as hydrogen storage, electrodes in electrochemical batteries and also as promising electrode materials in EC's [26].

In this study RF aerogels were synthesised through polycondensation reaction between resorcinol (R) and formaldehyde (F) followed by the carbonisation of the gels under Ar and finally physical activation of the carbons under $CO_2$ at different temperatures. Both resultant carbon and activated carbon aerogels were used as electroactive material for the fabrication of electrodes for EC's. Abbas et al. have previously shown that optimum pore size for maximum capacitance of supercapacitor cell using 6M KOH solution as electrolyte is in the range of 2nm [27]. In this activated carbons with pore size around 2nm were prepared at elevated temperatures under $CO_2$ atmosphere to increase their specific surface area and introduce the surface functional groups on their internal surface concomitantly. Influence of the introduction of oxygen functional groups on the wettability of the electrodes by electrolyte and their specific capacitance was evaluated. Contact angle measurements using different probe solutions was used to investigate the wettability of the carbon materials while their specific capacitance was determined by cyclic voltammetry (CV) and their resistive behaviour was assessed by electrochemical impedance spectroscopy (EIS) measurements in a two-electrode symmetrical cell using 6M KOH aqueous solution as electrolyte.

## 2. Experimental

### *2.1 Synthesis of RF gels*

The resorcinol/ formaldehyde (RF) aerogels were synthesised by polycondensation of resorcinol and formaldehyde with resorcinol / catalyst molar ratio of 100 according to the procedure explained elsewhere [28, 29].

### *2.2 Carbonization of RF aerogels (RFC)*

Samples of 3g vacuum dried RF polymeric gel were purged for 30 min with Ar at 30 ºC before commencement of carbonisation process. Gel samples were placed in middle of tubular furnace inside a ceramic boat and carbonized at 800 ºC before physical activation under $CO_2$ environment. Temperature was maintained at 150 ºC for 30 min after increasing it from room temperature at 5 ºC $min^{-1}$. The furnace temperature was further increased to 450 ºC at 5 ºC $min^{-1}$ and retained at 450 ºC for another 30 min before increasing it to the final carbonization temperature of 800 ºC at 10 ºC $min^{-1}$. The sample was then kept at 800 ºC for 3 hrs followed by cooling to room temperature. The entire process was performed under Ar flowing at 100 $cm^3$ $min^{-1}$.

### *2.3 RF aerogels activation (RFCA)*

Carbon samples were activated by physical activation at different temperatures using $CO_2$ as activation agent. Samples were first purged with Ar at 30 ºC before commencement of heating programme for 30 min. Temperature then was increased at 10 ºC $min^{-1}$ and the gas was switched from Ar to $CO_2$ once the desired activation temperature was achieved. The samples were kept at this temperature under $CO_2$ environment during the activation and then gas was switched back to Ar and the samples were cooled down to 30 ºC under Ar atmosphere.

### *2.4 surface cleaning of activated carbon aerogels (RFCA)*

3 grams of the sample RFCA100-800-800 was loaded in the ceramic boat, placed in the middle of the furnace and purged with Ar at 30 ºC for 30 min prior to heating. The temperature was then increased at a rate of 10 ºC $min^{-1}$ to 600 ºC and the sample was kept at this temperature for 1 hr followed by cooling down to 30 ºC. The entire process was performed under Ar flowing at 100 $cm^3$ $min^{-1}$.

### *2.5 Physical characterisation of carbon / activated carbon aerogels (RFC/RFCA)*

The porosity analysis of carbon (RFC) and activated carbon (RFCA) samples was performed by the analysis of nitrogen adsorption–desorption isotherms measured by Tri-Star adsorption analyser (Micromeritics). Samples were evacuated in vacuum oven at 80 ºC for 24 hrs followed by degassing at 300 ºC using a Flowprep system (Micrometrics) prior to the adsorption/desorption measurements. Surface area measurements were made using BET technique, micropore analysis was conducted using t-plot, and adsorption branch of the isotherm was used for pore size distribution using BJH method. The total pore volume was calculated from the adsorbed volume of $N_2$ at $P/P_0 = 0.99$ [29].

X-ray diffraction (XRD) was performed using a SIEMENS - D5000 X-ray diffractometer with the current and voltage kept at 30 mA and 40 kV respectively to analyse the morphological structure of carbon / activated carbon aerogels.

Raman spectroscopy was carried out on an "In via Raman microscope (Renishaw, UK)" with 514.5 nm diode laser excitation in the range of 500 – 2500 $cm^{-1}$ to evaluate the vibrational properties of carbon / activated carbon aerogels.

Fourier Transform Infrared Spectroscopy (Nicolet™ iS™ 50 FT-IR Spectrometer) was adopted to study the chemical composition of cleaned/ uncleaned activated carbon aerogels.

Measurements of surface properties of prepared samples were performed using X-Ray Photoelectron Spectroscopy (XPS) with the aid of a Specs Phoibos 100 MCD-5 (5 single channel electron multiplier) hemispherical analyser employing a Specs XR-50 X-ray source with Mg Kα (1253.6 eV) beam. All spectra were calibrated with respect to the binding energy of adventitious C1s peak at 284.8 eV. Measurements results were analysed in CasaXPS software.

CAM 200 goniometer system manufactured by KSV Ltd based on video captured images and automatic image analysis using CAM software was used to carry out Contact angle measurements. Deionised water, Ethylene glycol and Diiodomethane were used as probe liquid for the determination of contact angles.

### *2.6 Electrode fabrication*

Carbon/ activated carbon were extensively grinded to produce very fine power to prepare electrodes for electrochemical measurements. 80 wt% carbon / or activated carbon was mixed as active material with 10 wt% Cabot carbon black XC72 as conductivity enhancer and remaining 10% was Kynar 2801 as binder to fabricate the electrodes for the EC cell. The electrode constituents were mixed for 2 hours using magnetic stirrer to form a uniform paste using acetone as a solvent. The paste was rolled into uniform sheets with wet film thickness of 250 µm on aluminium foil using a micrometre adjustable applicator (RK Print Coat Instruments, Ltd.). Circular discs of 13mm diameter were punched out and kept at 85 ºC inside a vacuum oven overnight resulting in the electrodes with a dry thickness of approximately 100 micrometres.

### *2.7 Cell construction*

Pair of identical carbon / activated carbon electrodes casted on aluminium foil used as current collector, were used as cathode and anode electrodes in the EC cell. A glass micro fibre was used as separator to manufacture the symmetric sandwich type supercapacitor cell for electrochemical analysis as shown in Figure 1.

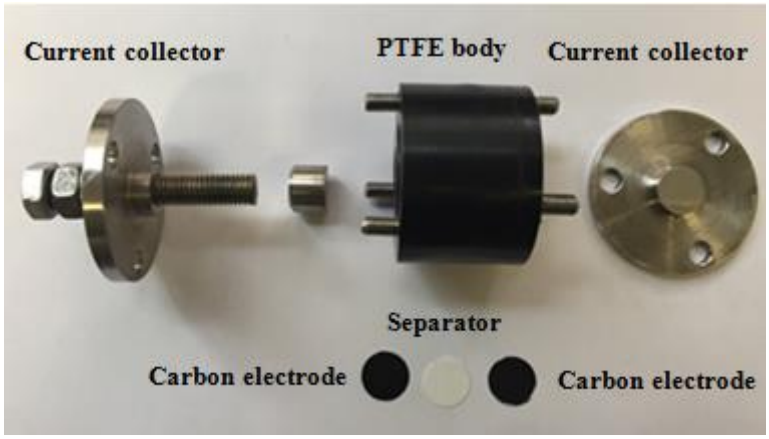


**Figure 1–** Sandwich type symmetric supercapacitor test cell

Central part of the test cell's body comprises of a corrosion resilient insulating PTFE. Upper current collector in the test cell is controlled by a stainless steel plunger which prevents any damage to carbon electrodes since it moves independently. The steel plunger is finger tighten to ensure a good contact between current collectors, electrodes and external plates. Glass fibre separator was soaked in 6M KOH electrolyte solution before its insertion between two carbon electrodes to ensure the availability of electrolyte. After assembling, the EC cell was placed under vacuum for 20 min prior to the electrochemical measurements to ensure the penetration of electrolyte solution through the porous structure of both electrodes.

### *2.8 Electrochemical characterisation*

Samples were electrochemically characterised using Voltalab 40 analytical potentiostat. The cell was kept under open circuit for 15 mins to stabilize prior to the electrochemical measurements. Cyclic voltammetry measurements were performed in a voltage range of 0.5 to 1.0 V at different scan rates between 5 and 15mV$s^{-1}$.

In this work 6M KOH was used as electrolyte solution and the specific capacitance of sandwich type symmetric capacitor cell was calculated from the discharge part of the CV curve using the following equation;

$$C = I \Big/ \left( \frac{dV}{dt} \right) \quad (1)$$

Where $I$ is the average discharge current and dV/dt is the scan rate.

The specific capacitance $C_{sp}$ in $Fg^{-1}$ was calculated by:

$$C_{sp} = 2 \times C / m \quad (2)$$

Where '$C$' is the measured specific capacitance for two-electrode cell and '$m$' is the mass of active material in each electrode.

The results of the characterization of carbons and activated carbons by different techniques and also their capacitive performance measured by cyclic voltammetry and electrochemical impedance spectroscopy when used as electroactive materials in EC cells are presented and discussed in the following section.

## 3. RESULTS AND DISCUSSION

In this section the results of different characterization techniques such as BET, XRD, XPS, FTIR, Raman spectroscopy and contact angle measurements to investigate the porosity development, introduction of surface functional groups, change in the morphology of carbons and their wettability with polar and non-polar probing liquids are presented. The effects of the modifications made to the carbon materials on the electrochemical performance of electrodes fabricated from these carbon samples are discussed.

### *3.1 BET analysis of carbon /activated carbon aerogels*

$N_2$ adsorption–desorption isotherms of the carbons and activated carbons at different activation temperatures are shown in Figure 2.

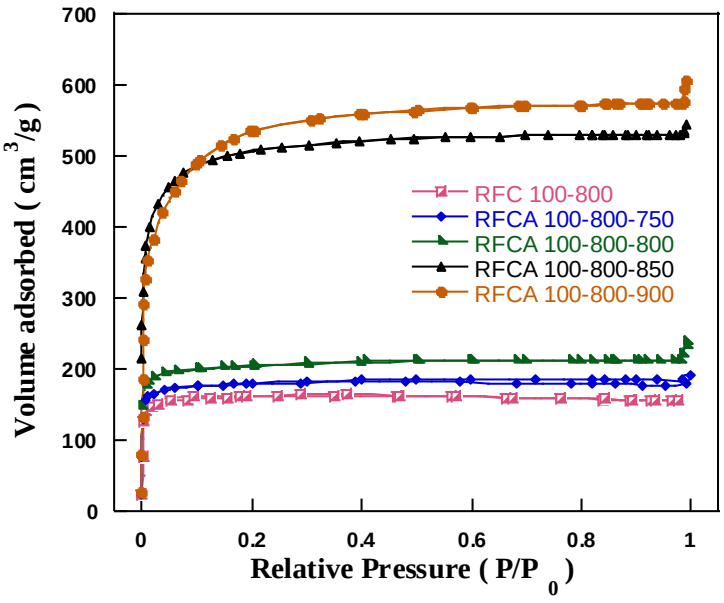


**Figure 2 –** $N_2$ adsorption–desorption isotherms of carbon / activated carbon aerogels.

The isotherms show a sharp increase in the amount of gas adsorbed at low pressures in the range of $P/P_0 < 0.01$ indicating the development of microporosity in carbon structure due to the physical activation. This is followed by a hysteresis loop in $P/P_0$ range 0.4-0.9 which represents the development of mesoporisity within the activated carbon samples [30]. The lower part of the hysteresis loops represent the filling of the mesopores while the upper parts represent the emptying of the mesopores [31]. With the increase in activation temperature the volume of gas adsorbed increases due to the development of porosity in the samples. Table.1 shows the results of porosity analysis where significant increase in pore volume and specific surface area can be observed with the average pore size remained constant around 2nm.

**Table 1** Porosity parameters of carbon/activated carbon aerogels.

| **Sample** | **$S_{BET}$** ($m^2g^{-1}$) | **$V_{total}$** ($cm^3g^{-1}$) | **$V_{micro}$** % | **$V_{meso}$** % | **$D_{avg}$** (nm) |
|---|---|---|---|---|---|
| RFC 100-800 | 537 | 0.2420 | 90 | 10 | 1.80 |
| RFCA 100-800-750 | 602 | 0.2981 | 79 | 21 | 1.99 |
| RFCA 100-800-800 | 678 | 0.3707 | 72 | 28 | 2.19 |
| RFCA 100-800-850 | 1687 | 0.8413 | 72 | 28 | 2.00 |
| RFCA100-800-900 | 1775 | 0.9394 | 42 | 58 | 2.12 |

Pore size distribution (PSD) of carbon / activated carbon aerogels is represented in Figure 3 indicating all samples are predominantly microporous in nature with a pore size distribution centred around 2 nm.

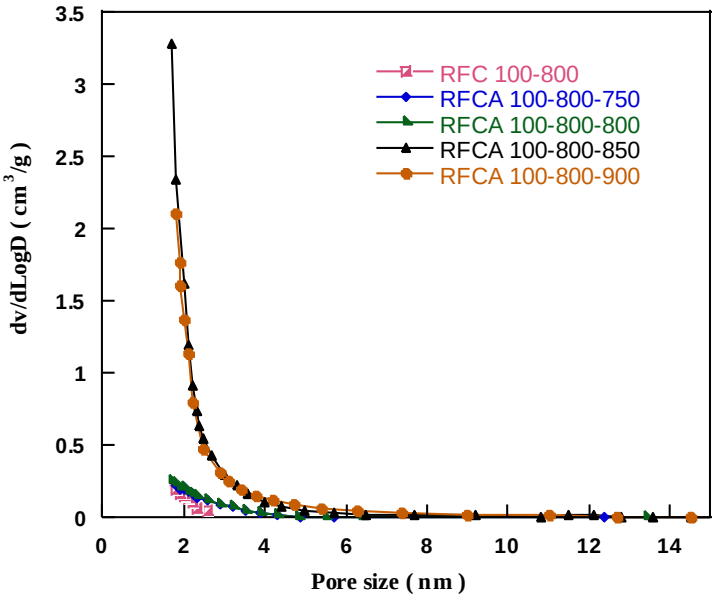


**Figure 3 –** Pore size distribution of carbon/activated carbon aerogels.

### *3.2 X-ray diffraction*

X-ray diffraction patterns of carbon / activated carbon aerogel samples shown in Figure 4 indicate two broad diffraction peaks around 2θ values of 23º and 44º. These peaks are assigned to (002) and (101) planes and represent the characteristic of an amorphous structure for the samples [32, 33]. The intensity of peak around 23º shows a significant decrease after activation indicating a decrease in the degree of graphitization of carbon with activation. Decrease in the degree of graphitization with activation temperature is further investigated by Raman spectroscopy and discussed in the next section [34].

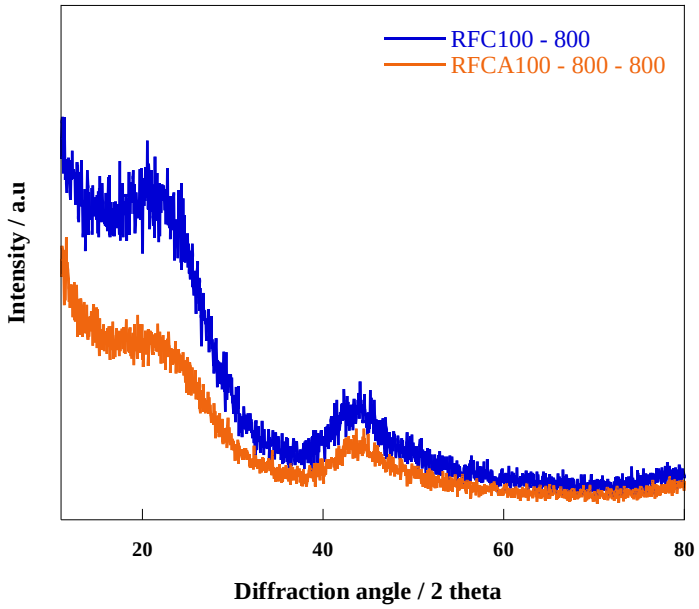


**Figure 4** –XRD spectrums of carbon/activated carbon aerogel samples.

### *3.3 Raman spectroscopy*

Figure 5 shows the Raman spectra of carbons activated at different temperatures. It is argued that activation results in a well-developed porous structure and increasing activation temperature and degree of burn off decreases the degree of graphitization [30]. Peaks around 1340 and 1600 $cm^{-1}$ on Raman spectra shown in Figure 5 are the characteristic peaks of such carbon materials [35]. The ratio of the relative intensity of the D and G bands ($I_D/I_G$) is proportional to the number of defect sites in carbon, where the higher the ratio is the lower the degree of graphitization [36].

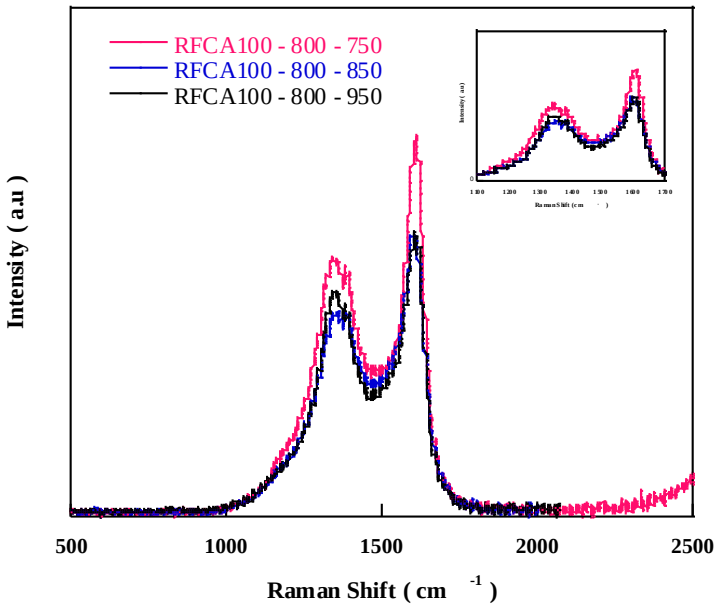

**Figure 5 –** Raman spectra of RFCA 100-800 activated at different temperatures.

Increase in activation temperature increases the $I_D$ / $I_G$ values which results in decrease in the degree of graphitization of carbon as listed in Table 2.

**Table 2** Raman features of activated carbons.

| Sample | Activation Temperature ($^oC$ ) | D Peak ($cm^{-1}$) | G Peak ($cm^{-1}$) | $I_D$ / $I_G$ |
|---|---|---|---|---|
| RFCA100 - 800 | 750 | 1340 | 1610 | 0.67 |
| RFCA100 - 800 | 850 | 1340 | 1590 | 0.72 |
| RFCA100 - 800 | 950 | 1350 | 1600 | 0.78 |

### *3.4 FTIR analysis*

The FTIR spectra in the range of wavenumbers from 500 to 4000 $cm^{-1}$ for both surface cleaned and uncleaned activated carbon aerogel samples are shown in Figure 6. Peaks present around 1590 and 1100 $cm^{-1}$ can be attributed to the carboxylic functional groups however the additional peak around 1530 $cm^{-1}$ on the spectrum of uncleaned activated carbon aerogel can be linked to asymmetric $NO_2$ [37-39]. Reduction in intensities or removal of bands around 1530 $cm^{-1}$ are due the thermal treatment applied during surface cleaning which results in removal of some surface groups and reduction in others for the surface cleaned (Sur-C) sample [40].

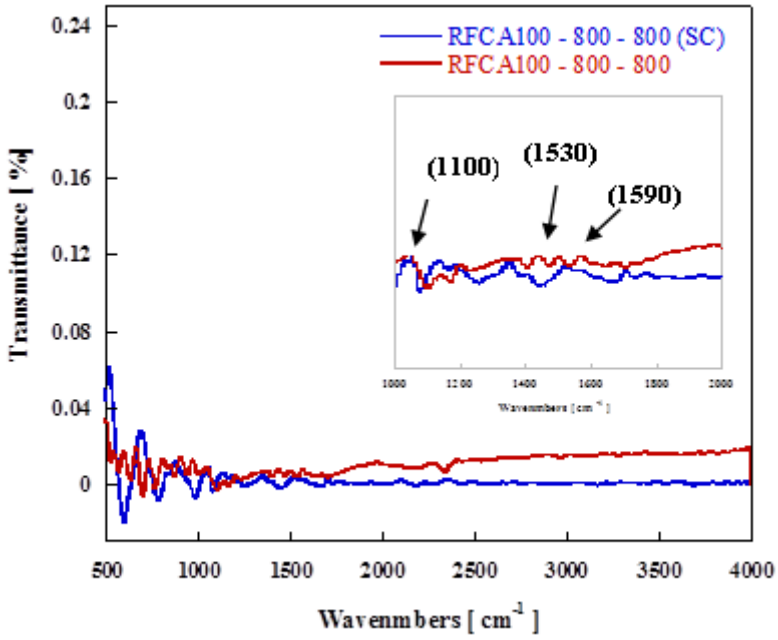


**Figure 6 –** FTIR spectra of surface cleaned and uncleaned activated carbon aerogel samples.

To understand the effect of surface functional groups on the performance of electrodes in an electrochemical cell, the surface of activated carbons was cleaned to remove the oxygen functional group introduced due to $CO_2$ activation.

### *3.5 X-Ray Photoelectron Spectroscopy (XPS)*

To understand the effect of surface functional groups on the performance of electrodes in an electrochemical cell, the surface of activated carbons was cleaned to remove the oxygen functional group introduced due to $CO_2$ activation.

The wide survey scan spectra of activated carbon and surface cleaned activated carbon samples are shown in Figure 7. The presence of the very strong peaks of F1s in both cases could be caused by using a polyvinylidene fluoride (Kynar 2801) as a binding material for the electrode.

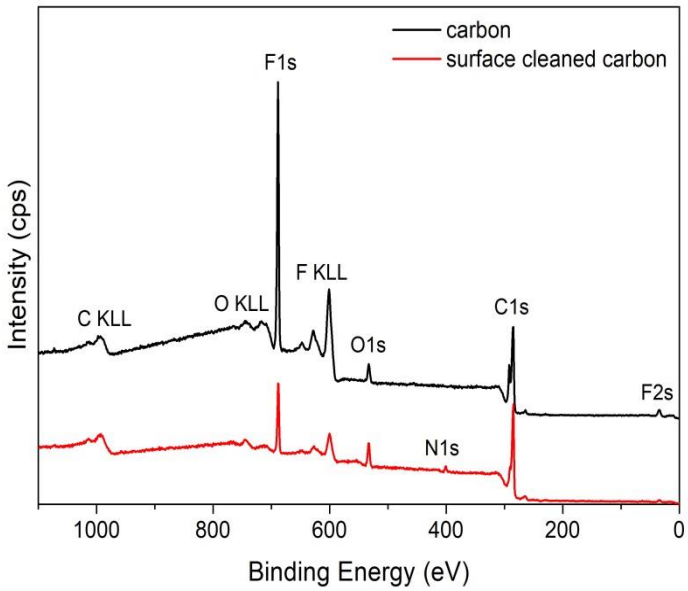


**Figure 7 –** Wide survey XPS scan of carbon (C) and surface cleaned carbon (SC) samples

The O1s spectra of both samples are shown in Figure 8 and it was observed that additional cleaning treatment did not influence on the O1s position, i.e. it was not shifted as-compared to uncleaned carbon sample. Spectra were de-convoluted into four components at ca. 531.7 eV, 532.6 eV, 533.7 eV and 535 eV. similarly Fan et al. [41] stated that the first component might be assigned to carboxyl (COO-) and oxygen double bound to carbon (O-C=O). A peak occurring at ca. 532.6 eV can be attributed to hydroxyl (C-OH) and carbonyl (C=O) function groups, while at ca. 533.7 eV to oxygen of aryl ethers (F -O- F) and oxygen singe bond in esters and carboxylic acids (O=C-O). In turn, the last peak that occurs at ca. 535 eV could be assigned to chemisorbed oxygen in carboxylic groups or water (H-O-H) [41].

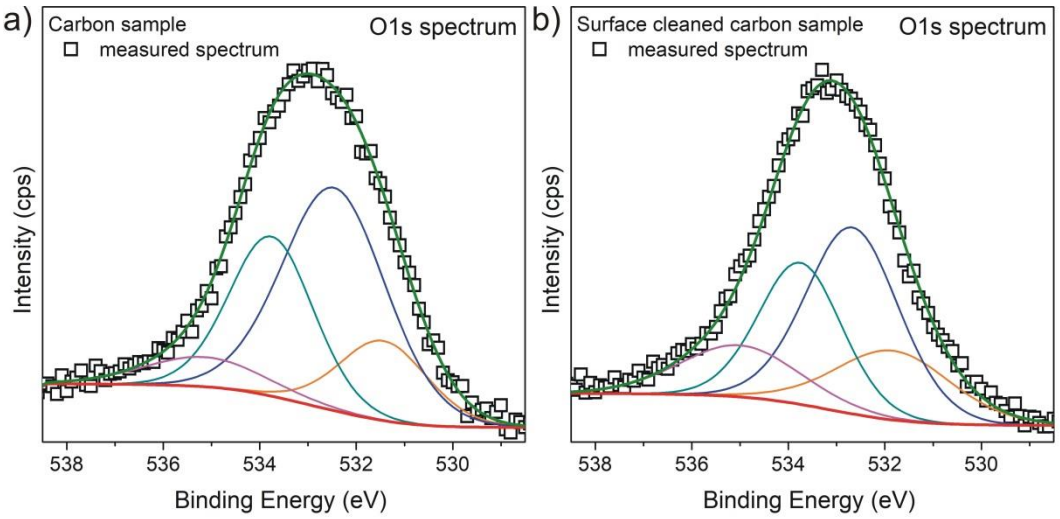


**Fig. 8**– O1s spectra of: a) carbon and b) surface cleaned carbon samples

A comparison of the spectra of cleaned and un-cleaned samples shows that the intensities of the de-convoluted spectra corresponded to different functional groups are decreased with surface cleaning. The results of this comparison are given in Table 3 in the form of mole% of C, N and O.

**Table 3** Elemental analysis (mol %) of activated carbon and surface cleaned activated carbon determined with the use of XPS method

| Sample | C | N | O | N/C | O/C |
|---|---|---|---|---|---|
| Activated Carbon | 86.64 | 2.91 | 10.45 | 0.034 | 0.121 |
| Surface cleaned activated | 92.74 | 0 | 7.26 | 0 | 0.078 |

Table 3 summarizes the elemental composition (C, O and N) of carbon and surface clean carbon samples obtained by XPS measurements. It is clearly seen that the oxygen content of uncleaned sample decreases from 10.45 mol% to 7.26 mol% after surface cleaning under inert conditions. This result indicates that surface cleaning at elevated temperatures under inert conditions led to the removal of oxygen functional groups from the surface.

### *3.6 Contact angle measurement*

Contact angle was found to be dependent on the type of substrate (carbon / activated carbon) and the probing liquid adopted as shown in Figure 9. The highest contact angle was observed

when most polar liquid (deionized water) was used as probing liquid on the carbon substrate. A significant decrease in the contact angle was observed when carbon substrate was substituted with the activated carbon aerogels. When ethylene glycol and Diiodomethane were used as probe liquids similar trends were observed. This decrease in contact angle can be attributed to the activation under $CO_2$ environment since it modifies the carbon surface by the introduction of oxygen functional groups [41].

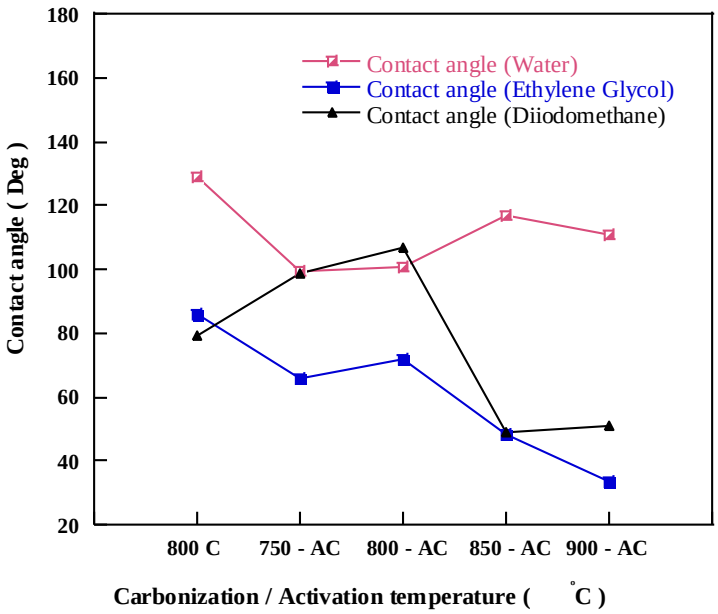


**Figure 9–** Contact angle measurements of carbon/activated carbon aerogels using different probing liquids.

### *3.7 Electrochemical properties*

#### *3.7.1 Cyclic voltammetry*

Figure 10 shows typical the cyclic voltammograms (CV) of activated carbon aerogel (RFCA100-800-800) used as electrode in EC cell with 6M KOH solution as electrolyte at scan rates of 5, 10 and 15 $mVs^{-1}$. All activated carbon aerogels demonstrated outstanding electrochemical performance in the potential range of 0.5-1.0 V at the same scan rates with 6M KOH electrolyte solution with very symmetric and nearly rectangular shape CV curves indicating reversible charging/discharge process in this potential range. This represents the formation of electric double layer charging at the electrode / electrolyte interface [42].

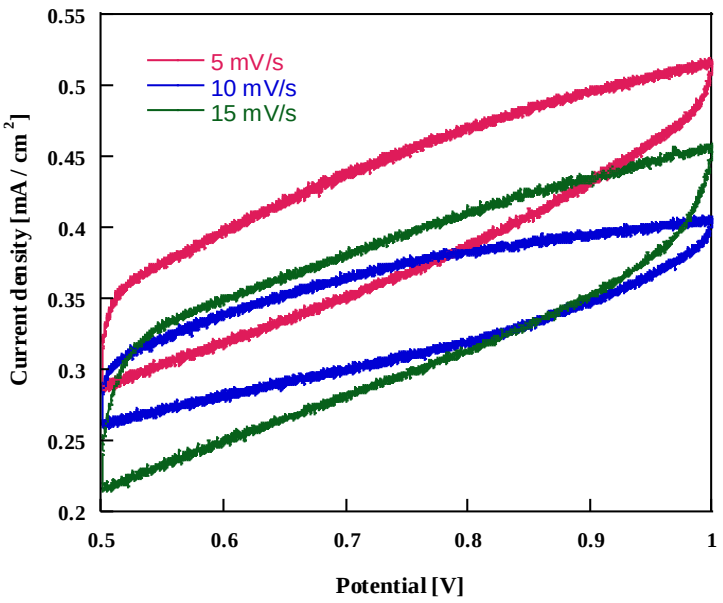


**Figure 10 –** Cyclic Voltammogram of the cell using (RFC100-800-900) activated carbon as the electroactive material at different scan rates.

The specific capacitance (SC) of the symmetrical EC cell calculated by discharge part of the CV curves for polymer based carbon and activated carbons activated at different temperatures are given in Table 4.

**Table 4** Specific capacitance of the electrodes at different scan rate in 6M KOH electrolyte

| **Sample** | **$S_{BET}$** ($m^2g^{-1}$) | **Specific Capacitance** ($Fg^{-1}$) Scan rate ($mVs^{-1}$) | | |
|---|---|---|---|---|
| | | 5 | 10 | 15 |
| RFC100 - 800 | 537 | 136 | 71 | 51 |
| RFCA100 – 800-750 | 602 | 144 | 52 | 23 |
| RFCA100 – 800-800 | 678 | 197 | 120 | 42 |
| RFCA100 – 800-800-(Sur-C) | 678 | 163 | 44 | 25 |
| RFCA100 – 800-850 | 1687 | 64 | 18 | 10 |
| RFCA100 – 800-850 | 1775 | 60 | 36 | 34 |

It can be seen that the carbon activated at 800 ºC delivers highest capacitance despite having a lower specific surface area (SSA) of 678 $m^2g^{-1}$ when compared with the carbon activated at 900 ºC having a SSA of 1775 $m^2g^{-1}$. This is mainly due to the collapse of the carbon nano-

structure at higher activation temperatures. This shows that optimizing micro / messo-porosity of the carbon plays a crucial role in achieving the highest specific capacitance.

*3.7.2 Electrochemical impedance spectroscopy (EIS)*

Electrochemical impedance spectroscopy was used to analyse the resistive behaviour and to approximate the capacitive performance of the electrode material.

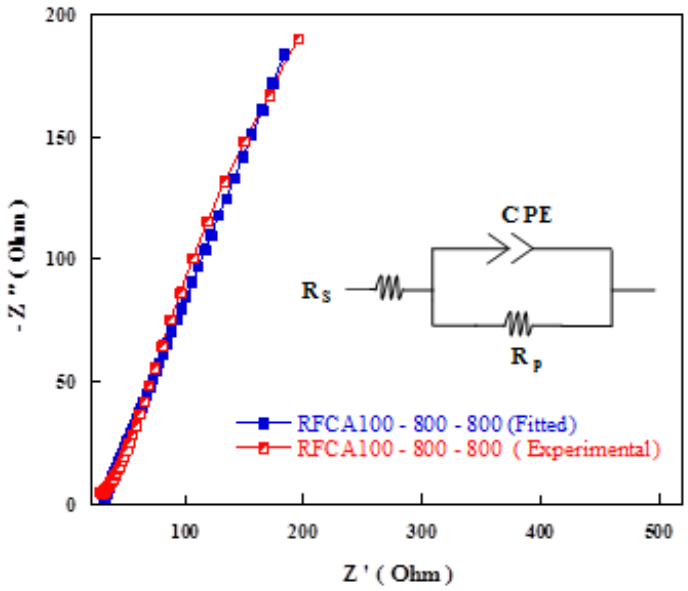


**Figure 11 –** EIS spectra of equivalent circuit fitting

An equivalent circuit used to fit EIS experimental data is shown in Figure 11 where experimental curve is in good agreement with the fitted curve. EIS parameters obtained by fitting the EIS data with the equivalent circuit model showed an increase in pore resistance from 8.12 **Ω** to 8.77 **Ω** after activation which could be due to the increased barrier to pore accessibility of the electrolyte. However a small decrease from 29.99 **Ω** to 29.59 **Ω** in solution resistance was witnessed which could be due to the improved wettability with increase in surface functional groups.

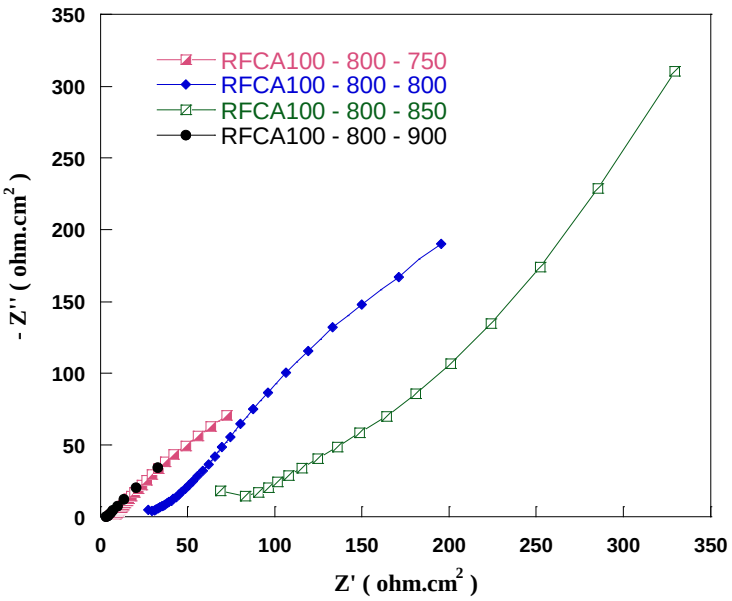


**Figure 12 –** EIS spectra of carbon aerogels with different activation temperature.

Figure 12 shows Nyquist plot for cell using activated carbons produced using different activation temperatures as electroactive material in the frequency range of 100 KHz to 50 Hz. Electrochemical capacitors behave like a resistor at very high frequencies (near the origin of the curve close to the Y-axis) however with the decrease in frequencies a sharp increase in the imaginary part of the resistance takes place and the curve becomes almost vertical due to the capacitive behaviour [45]. This indicates that by controlling the pore size and increasing the specific surface area through activation the capacitive behaviour of the electroactive material and final performance of the cell can be improved. In addition to this surface function groups also play a vital role to improve the electrode / electrolyte wettability which results in lower contact resistance and contribute towards the improved electrochemical performance of electrochemical cell.

## 4. Conclusions

Resorcinol / formaldehyde based carbon / activated carbon aerogels have been synthesised through polycondensation followed by carbonization and activation under Ar and $CO_2$ atmosphere respectively.

Effect of physical activation on the porosity of the carbon aerogels was assessed and it was observed that porosity was developed due to the activation process. Increase in the activation temperature resulted in increase in specific surface area while the average pore size remained

unchanged (around 2nm). Raman spectroscopy and XRD results showed that increasing the activation temperature results in decreasing the degree of graphitisation of carbon material.

The effect of the porous structure, wettability and surface functional groups on the specific capacitance of carbon electrodes in an EC cell was evaluated. Enhanced wettability and consequent increased specific capacitance was observed due to physical activation of polymeric carbons under $CO_2$ environment used as electroactive material. It was shown that the increased specific capacitance is mainly due to the increase in specific surface area and introduction of oxygen surface functional groups. Highest specific capacitance of 197 $Fg^{-1}$ at the scan rate of 5$mVs^{-1}$ was achieved using carbon activated at 800 ºC as an electrode active material. Carbon activated at 900 ºC with a SSA of 1775 $m^2g^{-1}$ showed a considerably lower capacitance where the marginal decrease in pore size was observed due to the collapse of the carbon nano-structure at higher activation temperatures. It is concluded that the pore size plays a key role on the capacitive behaviour of EC cell, with micropores contributing to the enhanced surface area and improved capacitance while mesopores provide path ways for the electrolyte and ion access within the carbon structure and internal surface.

Reduction in specific capacitance from 197 $Fg^{-1}$ to 163 $Fg^{-1}$ was observed after surface cleaning mainly due to the reduction in concentration of oxygen functional groups from10.45 mol% to 7.26 mol% in the activated carbon sample. EIS results also showed a reduction in the series due to the improved wettability of the carbon electrodes as a result of the introduction of oxygen functional groups with activation.

Electrochemical capacitors play a key role in energy storage systems when fast delivery and recovery of electric energy is required. However their low energy density has limited their capability and performance for a range of applications and improving the capacitive performance and energy density of ECs without sacrificing their power densities yet is a significant research challenge. This can be done through the introduction of functional groups such as oxygen or nitrogen on the surface of the electroactive materials or via the incorporation of nitrogen and oxygen heteroatoms within the structure of the materials. Use of metal oxides such as silver-oxide, $MnO_2$, ZnO and other metal oxides directly as electroactive material or as an doping pseudo-capacitive agents mixed with carbon can further enhanced the capacitive performance and energy density of ECs while maintaining their power capabilities. Although there is a direct relationship between the capacitance of the device and surface area of the electrode, however accessibility of the electrolyte to the internal surface area through porous

pathways play a key role in its final performance and therefore controlling the size of pores in-line with type of the electrolyte used is crucial.

## References


[1] A. Alaswad, A. Baroutaji, H. Achour, J. Carton, A. Al Makky, and A. Olabi, "Developments in fuel cell technologies in the transport sector," *International Journal of Hydrogen Energy,* vol. 41, pp. 16499-16508, 2016.

[2] T. Wilberforce, Z. El-Hassan, F. Khatib, A. Al Makky, A. Baroutaji, J. G. Carton*, et al.*, "Developments of electric cars and fuel cell hydrogen electric cars," *International Journal of Hydrogen Energy,* vol. 42, pp. 25695-25734, 2017.

[3] A. Olabi, "Renewable energy and energy storage systems," ed: Elsevier, 2017.

[4] X. Guo, B. Sun, D. Su, X. Liu, H. Liu, Y. Wang*, et al.*, "Recent developments of aprotic lithium-oxygen batteries: functional materials determine the electrochemical performance," *Science Bulletin,* 2017.

[5] P. J. Hall, M. Mirzaeian, S. I. Fletcher, F. B. Sillars, A. J. Rennie, G. O. Shitta-Bey*, et al.*, "Energy storage in electrochemical capacitors: designing functional materials to improve performance," *Energy & Environmental Science,* vol. 3, pp. 1238-1251, 2010.

[6] M. O. Yanik, E. A. Yigit, Y. E. Akansu, and E. Sahmetlioglu, "Magnetic conductive polymer-graphene nanocomposites based supercapacitors for energy storage," *Energy,* vol. 138, pp. 883-889, 2017.

[7] L. Xu, Y. Zhao, J. Lian, Y. Xu, J. Bao, J. Qiu*, et al.*, "Morphology controlled preparation of ZnCo 2 O 4 nanostructures for asymmetric supercapacitor with ultrahigh energy density," *Energy,* vol. 123, pp. 296-304, 2017.

[8] J.-j. Ruan, Y.-q. Huo, and B. Hu, "Three-dimensional Ni (OH) 2/Cu 2 O/CuO porous cluster grown on nickel foam for high performance supercapacitor," *Electrochimica Acta,* vol. 215, pp. 108-113, 2016.

[9] D. Xiang, L. Yin, C. Wang, and L. Zhang, "High electrochemical performance of RuO 2–Fe 2 O 3 nanoparticles embedded ordered mesoporous carbon as a supercapacitor electrode material," *Energy,* vol. 106, pp. 103-111, 2016.

[10] A. Lahyani, P. Venet, A. Guermazi, and A. Troudi, "Battery/supercapacitors combination in uninterruptible power supply (UPS)," *IEEE transactions on power electronics,* vol. 28, pp. 1509-1522, 2013.

[11] Y. Zhan, Y. Guo, J. Zhu, and L. Li, "Power and energy management of grid/PEMFC/battery/supercapacitor hybrid power sources for UPS applications," *International Journal of Electrical Power & Energy Systems,* vol. 67, pp. 598-612, 2015.

[12] P. Coenen, F. Leemans, and G. Mulder, "Applying large electric double layer capacitor systems," *Journal of Applied Electrochemistry,* vol. 44, pp. 533-542, 2014.

[13] N. Jäckel, D. Weingarth, A. Schreiber, B. Krüner, M. Zeiger, A. Tolosa*, et al.*, "Performance evaluation of conductive additives for activated carbon supercapacitors in organic electrolyte," *Electrochimica Acta,* vol. 191, pp. 284-298, 2016.

[14] T. Rath, N. Pramanik, and S. Kumar, "High electrochemical performance flexible solid-state supercapacitor based on Co-doped reduced graphene oxide and silk fibroin composites," *Energy,* 2017.

[15] W. Christinelli, L. da Trindade, A. Trench, C. Quintans, C. Paranhos, and E. Pereira, "High-performance energy storage of poly (o-methoxyaniline) film using an ionic liquid as electrolyte," *Energy,* 2017.

[16] Y. Zhu, S. Murali, M. D. Stoller, K. Ganesh, W. Cai, P. J. Ferreira*, et al.*, "Carbon-based supercapacitors produced by activation of graphene," *Science,* vol. 332, pp. 1537-1541, 2011.

[17] J. Chmiola, G. Yushin, Y. Gogotsi, C. Portet, P. Simon, and P.-L. Taberna, "Anomalous increase in carbon capacitance at pore sizes less than 1 nanometer," *Science,* vol. 313, pp. 1760-1763, 2006.

[18] Q. Abbas, M. Mirzaeian, and A. A. Ogwu, "Electrochemical performance of controlled porosity resorcinol/formaldehyde based carbons as electrode materials for supercapacitor applications," *International Journal of Hydrogen Energy,* 2017.

[19] S. L. Candelaria, B. B. Garcia, D. Liu, and G. Cao, "Nitrogen modification of highly porous carbon for improved supercapacitor performance," *Journal of Materials Chemistry,* vol. 22, pp. 9884-9889, 2012.

[20] S. Majid, "Effects of Electrodeposition Mode and Deposition Cycle on the Electrochemical Performance of MnO 2-NiO Composite Electrodes for High-Energy-Density Supercapacitors," *PloS one,* vol. 11, p. e0154566, 2016.

[21] Z. Li, P. Liu, G. Yun, K. Shi, X. Lv, K. Li*, et al.*, "3D (Three-dimensional) sandwich-structured of ZnO (zinc oxide)/rGO (reduced graphene oxide)/ZnO for high performance supercapacitors," *Energy,* vol. 69, pp. 266-271, 2014.

[22] B. Patil, S. Ahn, C. Park, H. Song, Y. Jeong, and H. Ahn, "Simple and novel strategy to fabricate ultra-thin, lightweight, stackable solid-state supercapacitors based on MnO2-incorporated CNT-web paper," *Energy,* vol. 142, pp. 608-616, 2018.

[23] B. Conway, V. Birss, and J. Wojtowicz, "The role and utilization of pseudocapacitance for energy storage by supercapacitors," *Journal of Power Sources,* vol. 66, pp. 1-14, 1997.

[24] D. Hulicova, J. Yamashita, Y. Soneda, H. Hatori, and M. Kodama, "Supercapacitors prepared from melamine-based carbon," *Chemistry of Materials,* vol. 17, pp. 1241-1247, 2005.

[25] M. Mirzaeian, Q. Abbas, A. Ogwu, P. Hall, M. Goldin, M. Mirzaeian*, et al.*, "Electrode and electrolyte materials for electrochemical capacitors," *International Journal of Hydrogen Energy,* 2017.

[26] A. Eftekhari and B. Fang, "Electrochemical hydrogen storage: Opportunities for fuel storage, batteries, fuel cells, and supercapacitors," *International Journal of Hydrogen Energy,* 2017.

[27] Q. Abbas, M. Mirzaeian, and A. A. Ogwu, "Electrochemical performance of controlled porosity resorcinol/formaldehyde based carbons as electrode materials for supercapacitor applications," *International Journal of Hydrogen Energy,* vol. 42, pp. 25588-25597, 2017.

[28] M. Mirzaeian and P. J. Hall, "The control of porosity at nano scale in resorcinol formaldehyde carbon aerogels," *Journal of materials science,* vol. 44, pp. 2705-2713, 2009.

[29] M. Mirzaeian and P. J. Hall, "Nano structure carbons for energy storage in lithium oxygen batteries," in *Sustainable Power Generation and Supply, 2009. SUPERGEN'09. International Conference on*, 2009, pp. 1-10.

[30] M. Zhou, F. Pu, Z. Wang, and S. Guan, "Nitrogen-doped porous carbons through KOH activation with superior performance in supercapacitors," *Carbon,* vol. 68, pp. 185-194, 2014.

[31] S. J. Gregg, K. S. W. Sing, and H. Salzberg, "Adsorption surface area and porosity," *Journal of The Electrochemical Society,* vol. 114, pp. 279C-279C, 1967.

[32] D. P. Dubal, N. R. Chodankar, Z. Caban-Huertas, F. Wolfart, M. Vidotti, R. Holze*, et al.*, "Synthetic approach from polypyrrole nanotubes to nitrogen doped pyrolyzed carbon nanotubes for asymmetric supercapacitors," *Journal of Power Sources,* vol. 308, pp. 158-165, 2016.

[33] N. S. M. Nor, M. Deraman, R. Omar, R. Farma, N. H. Basri, B. N. M. Dolah*, et al.*, "Influence of gamma irradiation exposure on the performance of supercapacitor electrodes made from oil palm empty fruit bunches," *Energy,* vol. 79, pp. 183-194, 2015.

[34] J. Zhu, Y. Xu, Y. Zhang, T. Feng, J. Wang, S. Mao*, et al.*, "Porous and high electronic conductivity nitrogen-doped nano-sheet carbon derived from polypyrrole for high-power supercapacitors," *Carbon,* vol. 107, pp. 638-645, 2016.

[35] M. Zhou, T. Cai, F. Pu, H. Chen, Z. Wang, H. Zhang*, et al.*, "Graphene/carbon-coated Si nanoparticle hybrids as high-performance anode materials for Li-ion batteries," *ACS applied materials & interfaces,* vol. 5, pp. 3449-3455, 2013.

[36] M. Liu, L. Gan, W. Xiong, F. Zhao, X. Fan, D. Zhu*, et al.*, "Nickel-doped activated mesoporous carbon microspheres with partially graphitic structure for supercapacitors," *Energy & Fuels,* vol. 27, pp. 1168-1173, 2013.

[37] S. Biniak, G. Szymański, J. Siedlewski, and A. Światkowski, "The characterization of activated carbons with oxygen and nitrogen surface groups," *Carbon,* vol. 35, pp. 1799-1810, 1997.

[38] T. J. Bandosz and C. Ania, "Surface chemistry of activated carbons and its characterization," *Interface Science and Technology,* vol. 7, pp. 159-229, 2006.

[39] J. Zawadzki, "IR spectroscopy in carbon surface chemistry," *Chemistry and physics of carbon,* vol. 21, pp. 180-200, 1989.

[40] M. Seredych, D. Hulicova-Jurcakova, G. Q. Lu, and T. J. Bandosz, "Surface functional groups of carbons and the effects of their chemical character, density and accessibility to ions on electrochemical performance," *Carbon,* vol. 46, pp. 1475-1488, 2008.

[41] L.-Z. Fan, S. Qiao, W. Song, M. Wu, X. He, and X. Qu, "Effects of the functional groups on the electrochemical properties of ordered porous carbon for supercapacitors," *Electrochimica Acta,* vol. 105, pp. 299-304, 2013.

[42] L. Sui, Y. Wang, W. Ji, H. Kang, L. Dong, and L. Yu, "N-doped ordered mesoporous carbon/graphene composites with supercapacitor performances fabricated by evaporation induced self-assembly," *International Journal of Hydrogen Energy,* 2017.

[43] L. Zhang, H. Liu, M. Wang, and L. Chen, "Structure and electrochemical properties of resorcinol–formaldehyde polymer-based carbon for electric double-layer capacitors," *Carbon,* vol. 45, pp. 1439-1445, 2007.

[44] B. Xu, Y. Chen, G. Wei, G. Cao, H. Zhang, and Y. Yang, "Activated carbon with high capacitance prepared by NaOH activation for supercapacitors," *Materials Chemistry and Physics,* vol. 124, pp. 504-509, 2010.

[45] M. J. Mostazo-López, R. Ruiz-Rosas, E. Morallón, and D. Cazorla-Amorós, "Nitrogen doped superporous carbon prepared by a mild method. Enhancement of supercapacitor performance," *international journal of hydrogen energy,* vol. 41, pp. 19691-19701, 2016.